Metallophysics and Advanced Technologies
Металофіз. новітні технол.
Metallofiz. Noveishie Tekhnol.
2025, vol. 47, No. 11, pp. 1239–1256
https://doi.org/10.15407/mfint.47.11.1239
Reprints available directly from the publisher

PACS numbers: 46.40.-f, 46.50.+a, 61.43.Gt, 62.20.mj, 62.20.mm, 62.30.+d, 81.05.Rm

Parametric Investigations on Dynamic Responses of Porous Functionally Graded Al/Al_2O_3 Plates: Effects of Homogenization Models and Material Distributions

M. Hadji, B. Rebai[*], M. Rabehi[**], M. Meradjah[***,****], and T. Messas[*]

Climatic Engineering Department, Faculty of Sciences and Technology,
University of Brothers Mentouri Constantine 1,
Constantine, Algeria
[*]*Civil Engineering Department, Faculty of Sciences and Technology,*
Abbes Laghrour University,
Khenchela, Algeria
[**]*Abdelhafid Boussouf University,*
Mila, Algeria
[***]*Civil Engineering Department, Faculty of Technology,*
University of Sidi Bel Abbes,
Algeria
[****]*Multiscale Modelling and Simulation Laboratory of Sidi Bel Abbes,*
Algeria

This study analyses numerically the dynamic responses of functionally graded Al/Al_2O_3 plates with porosity. It investigates the effects of key parameters including thickness-to-span ratio and porosity coefficient on the non-dimensional fundamental frequencies. Various micromechanical homogenization models (by Voigt, Mori–Tanaka, LRVE, Tamura, Reuss) are applied across different-material volume-fraction distribution profiles (power-law, Viola–Tornabene four-parameters', trigonometric ones). Four porosity-variation patterns are considered: even, uneven, logarithmic-uneven, and mass-density. The Navier solution technique is employed to solve the govern-

Corresponding author: Malek Hadji
E-mail: malekhadji25@gmail.com

Citation: M. Hadji, B. Rebai, M. Rabehi, M. Meradjah, and T. Messas, Parametric Investigations on Dynamic Responses of Porous Functionally Graded Al/Al_2O_3 Plates: Effects of Homogenization Models and Material Distributions, *Metallofiz. Noveishie Tekhnol.*, **47**, No. 11: 1239–1256 (2025). DOI: 10.15407/mfint.47.11.1239

ing equations. Results show that the Viola–Tornabene model produces the highest frequencies, followed by power-law and trigonometric models. Mass-density porosity yields maximum frequencies, while even porosity gives minimum values. Increasing porosity coefficient generally increases frequencies, except for even porosity. Increasing thickness-to-span ratio decreases frequencies across all models. The findings provide insights for optimizing functionally graded porous plate designs.

Key words: functionally graded materials, elastic foundations, homogenization models, dynamic response, porosity, fundamental frequencies.

В роботі проведено числову аналізу динамічних параметрів відгуків функціонально ґрадієнтних пористих пластин Al/Al_2O_3. Досліджено вплив ключових параметрів, зокрема відношення товщини до довжини прольоту та коефіцієнта пористости, на безрозмірні основні частоти. Різні моделі мікромеханічної гомогенізації (за Фохтом, Морі–Танаки, LRVE, Тамурою, Райссом) застосовано до різних профілів розподілу об'ємної частки матеріялу (степеневого, чотирипараметричного Віоли–Торнабене, тригонометричного). Розглянуто чотири моделі зміни пористости: парний, непарний, логаритмічно-непарний і масово-щільний. Для розв'язання керівних рівнянь використовується метод розв'язання за Нав'є. Результати показують, що модель Віоли–Торнабене дає найвищі частоти; за нею йдуть степеневі та тригонометричні моделі. Масово-щільна пористість дає максимальні частоти, тоді як парна пористість дає мінімальні значення. Збільшення коефіцієнта пористости зазвичай збільшує частоти, за винятком випадку парної пористости. Збільшення відношення товщини до довжини прольоту понижує частоти у всіх моделях. Одержані результати дають уявлення про оптимізацію конструкцій функціонально ґрадієнтних пористих пластин.

Ключові слова: функціонально ґрадієнтні матеріяли, пружність, моделі гомогенізації, динамічний відгук, пористість, основні частоти.

(Received 1 August, 2024; in final version, 27 August, 2024)

1. INTRODUCTION

Functionally graded (FG) materials (FGMs) have gained significant attention in engineering applications due to their ability to exhibit spatially varying properties. These materials offer advantages in terms of thermal resistance, reduced residual and thermal stresses, and improved fracture toughness. The introduction of porosity in FGMs can further improve their performance by reducing weight and modifying mechanical properties.

This study focuses on the dynamic behaviour of functionally graded Al/Al_2O_3 plates with porosity. The analysis of such structures is crucial for their effective design and application in various fields, including aerospace, automotive, and civil engineering [1–3].

Various research endeavours have contributed significantly to this domain. Addou *et al.* investigated the dynamic response of functionally graded plates resting on Winkler–Pasternak–Kerr foundations with varying porosity levels [4]. Their study, employing a simple quasi-3D hyperbolic theory, scrutinized the influences of gradient index, porosity, foundation stiffness, mode numbers, and geometry on natural frequencies. Similarly, Zaoui *et al.* conducted flexural analysis on FG plates supported by elastic foundations, employing novel 2D and quasi-3D higher-order shear deformation theories [5].

Furthermore, the collective contributions of Damani *et al.*, Merdaci *et al.*, and Mahmoudi *et al.* have enriched the field by investigating various aspects of porous FG plates, including bending, vibration, and dynamic analysis. They employed diverse shear deformation theories and examined the effects of different parameters on mechanical behaviour. Similarly, the works of Berkia *et al.*, Billel, and Benaddi *et al.* have significantly advanced the understanding of FGM and nanoplates. Their research includes the effects of parametric homogenization models such as by Reuss, LRVE, and Tamura ones on natural frequency, axial, and shear stress, and the factors influencing the vibration behaviour of FGM nanoplates [6–11].

Researchers have explored advanced computational techniques and homogenization models to conduct accurate analyses of porous FG plates. Yin *et al.* introduced a scaled boundary finite element method for bending and free vibration analyses [12]. Al Rjoub and Alshatnawi utilized artificial neural networks to predict natural frequencies [13], while Hu and Fu delved into the intricate effects of porosity distribution and grading patterns on the free vibration response of FG plates [14]. Kaddari *et al.* investigated the statics and free vibration of FG porous plates on elastic foundations, employing a novel quasi-3D hyperbolic shear deformation theory [15].

Additional studies have further expanded our understanding of porous FG structures.

Sharma *et al.* introduced a 3D degenerated shell element approach for free vibration analysis [16]. Sah and Ghosh explored the free vibration and buckling behaviour of multi-directional porous FG sandwich plates [17], while Kumar *et al.* conducted free vibration analyses of tapered FG plates with porosity [18,19]. Shahsavari *et al.* proposed a novel quasi-3D hyperbolic theory for free vibration analysis of FG porous plates on elastic foundations [20].

Researchers utilize various mathematical laws to describe the spatial variation of material properties in FGMs, including exponential [21], sigmoid [22], and power-law [23] distributions. Further studies have examined aspects such as elastic buckling, vibration response, and thermal behaviour of porous FG structures [24–31].

The present work aims to provide a comprehensive analysis of the dynamic responses of porous functionally graded plates by considering various factors: different micromechanical homogenization models (by Voigt, Mori–Tanaka, LRVE, Tamura, Reuss), material volume fraction distribution profiles (power-law, Viola–Tornabene four-parameter, trigonometric ones), porosity variation patterns (even, uneven, logarithmic-uneven, mass-density ones), effects of thickness-to-span ratio and porosity coefficient.

By employing the Navier solution technique and conducting parametric studies, this research seeks to offer valuable insights into the behaviour of porous FGM plates under dynamic loading conditions. The findings of this study will contribute to the optimization of FGM designs for various engineering applications.

2. THEORETICAL FORMULATIONS

2.1. Geometry and Material Properties

We examine an isotropic functionally graded rectangular plate made of a porous material whose properties vary in the thickness direction. The plate has thickness h, length a, and width b. A co-ordinate system $O(x, y, z)$ is defined with the origin at one corner of the mid-plane of the plate, as shown in Fig. 1, *a*. The edges of the plate are aligned with the x and y axes. The plate material is isotropic in the (xy) plane.

The plate has isotropic material properties $P(z)$ that vary through the thickness direction z. Two key properties, Young's modulus $E(z)$ and mass density $\rho(z)$, follow a power law distribution:

$$P(z) = P_{\mathrm{b}} + (P_{\mathrm{t}} - P_{\mathrm{b}})\left(\frac{1}{2} + \frac{z}{h}\right)^{\Delta} - \Xi(\phi), \tag{1}$$

where $P_{\mathrm{b}}(z)$ are the values at the bottom face and $P_{\mathrm{t}}(z)$ are the values at the top face. The exponent Δ is a gradient index that controls how rapidly the properties change through the thickness. The porosity varies through the thickness based on a distribution function $\Xi(\phi)$. We examine two specific forms for $\Xi(\phi)$ determined by a porous coefficient ϕ $(0 \le \phi < 0.5)$ as shown in Fig. 2:
evenly distributed porosities P1 with

$$\Xi(\phi) = \phi(P_{\mathrm{t}} + P_{\mathrm{b}}) / 2 ; \tag{2}$$

unevenly distributed porosities P2 with

$$\Xi(\phi) = \frac{\phi}{2}(P_{\mathrm{t}} + P_{\mathrm{b}})\left(1 - \frac{2|z|}{h}\right). \tag{3}$$

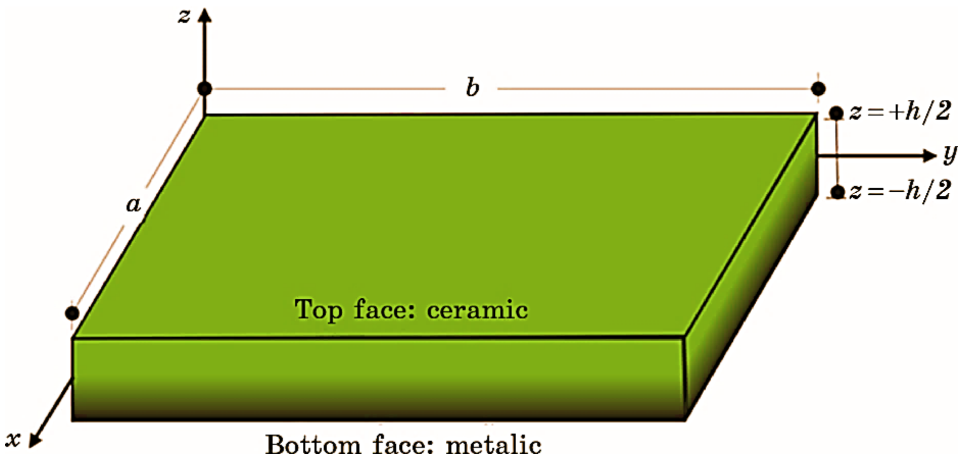

Fig. 1. Co-ordinates and geometry notation.

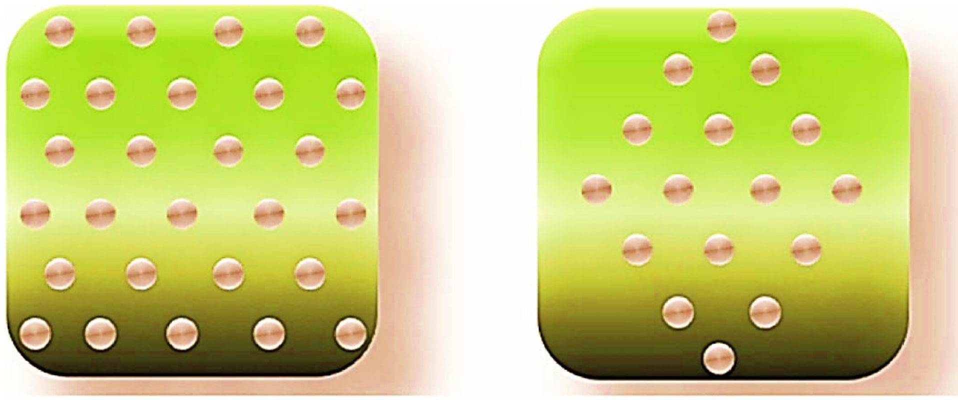

Fig. 2. Illustration of different patterns of porosity variations: evenly distributed porosities P1 (a), unevenly distributed porosities P2 (b).

2.2. Displacement Field

The four-variable hyperbolic quasi-3D shear deformation theory (FHQSDT) proposes a mathematical model for describing the displacement behaviour of FG plates u_i ($i = 1, 2, 3$):

$$u_1(x, y, z) = u_{0.1}(x, y) - z\frac{\partial u_{0.3}(x, y)}{\partial x} + \Phi(z)\frac{\partial u_{0.4}(x, y)}{\partial x},$$

$$u_2(x, y, z) = u_{0,2}(x, y) - z\frac{\partial u_{0.3}(x, y)}{\partial y} + \Phi(z)\frac{\partial u_{0.4}(x, y)}{\partial y}, \quad (4)$$

$$u_3(x,y,z) = u_{0.3}(x,y) + \Gamma(z)\, u_{0.4}(x,y),$$

where $u_{0.1}(x, y)$, $u_{0.2}(x, y)$, $u_{0.3}(x, y)$, and $u_{0.4}(x, y)$ are displacements in the directions of x, y, and z, $\Phi(z)$ and $\Gamma(z)$ are the shape functions in the longitudinal and transverse shear displacement distributions respectively with the following expressions for $\Phi(z)$ and $\Gamma(z)$:

$$\Phi(z) = \frac{z\,\mathrm{sech}(2z/h)}{h} - \frac{z(1-\mathrm{th}\,1)}{h\,\mathrm{ch}\,1}, \tag{5}$$

$$\Gamma(z) = \frac{1}{3h}\mathrm{sech}\left(\frac{2z}{h}\right)\left(1 - \frac{2z}{h}\mathrm{th}\left(\frac{2z}{h}\right) - \mathrm{ch}\left(\frac{2z}{h}\right)\frac{1-\mathrm{th}\,1}{\mathrm{ch}\,1}\right). \tag{6}$$

2.3. Stress–Strain Relationship

With small plate strains assumed, strains are related to displacements and their derivatives through an equation. This connects the displacement field to strains as follow:

$$\begin{aligned} \bar{\varepsilon} &= \{\varepsilon_{xx}\ \varepsilon_{yy}\ \gamma_{xy}\ \varepsilon_{zz}\}^{\mathrm{T}} = \bar{\varepsilon}_1 + \bar{\varepsilon}_2 z + \Phi(z)\bar{\varepsilon}_3 + \frac{\partial\Gamma(z)}{\partial z}\bar{\varepsilon}_4, \\ \bar{\gamma} &= \{\gamma_{xz}\ \gamma_{yz}\}^{\mathrm{T}} = \left(\frac{\partial\Phi(z)}{\partial z} + \Gamma(z)\right)\bar{\varepsilon}_5, \end{aligned} \tag{7}$$

in which

$$\bar{\varepsilon}_1 = \begin{Bmatrix} \dfrac{\partial u_{0.1}}{\partial x} \\ \dfrac{\partial u_{0.2}}{\partial y} \\ \dfrac{\partial u_{0.1}}{\partial y} + \dfrac{\partial u_{0.2}}{\partial x} \\ 0 \end{Bmatrix},\ \bar{\varepsilon}_2 = \begin{Bmatrix} \dfrac{\partial^2 u_{0.3}}{\partial x^2} \\ \dfrac{\partial^2 u_{0.3}}{\partial y^2} \\ 2\dfrac{\partial^2 u_{0.3}}{\partial x\partial y} \\ 0 \end{Bmatrix},\ \bar{\varepsilon}_3 = \begin{Bmatrix} \dfrac{\partial^2 u_{0.4}}{\partial x^2} \\ \dfrac{\partial^2 u_{0.4}}{\partial y^2} \\ 2\dfrac{\partial^2 u_{0.4}}{\partial x\partial y} \\ 0 \end{Bmatrix},$$

$$\bar{\varepsilon}_4 = \begin{Bmatrix} 0 \\ 0 \\ 0 \\ u_{0.4} \end{Bmatrix},\ \bar{\varepsilon}_5 = \begin{Bmatrix} \dfrac{\partial u_{0.4}}{\partial x} \\ \dfrac{\partial u_{0.4}}{\partial y} \end{Bmatrix}. \tag{8}$$

For linear elastic FG plates, Hooke's law relates stresses to strains through elastic coefficients. The coefficients vary continuously across the plate thickness:

$$\begin{Bmatrix} \sigma_{xx} \\ \sigma_{yy} \\ \sigma_{zz} \\ \tau_{yz} \\ \tau_{xz} \\ \tau_{xy} \end{Bmatrix} = \begin{bmatrix} Q_{11}(z) & Q_{12}(z) & Q_{13}(z) & 0 & 0 & 0 \\ Q_{12}(z) & Q_{22}(z) & Q_{23}(z) & 0 & 0 & 0 \\ Q_{13}(z) & Q_{23}(z) & Q_{33}(z) & 0 & 0 & 0 \\ 0 & 0 & 0 & Q_{44}(z) & 0 & 0 \\ 0 & 0 & 0 & 0 & Q_{55}(z) & 0 \\ 0 & 0 & 0 & 0 & 0 & Q_{66}(z) \end{bmatrix} \begin{Bmatrix} \varepsilon_{xx} \\ \varepsilon_{yy} \\ \varepsilon_{zz} \\ \gamma_{yz} \\ \gamma_{xz} \\ \gamma_{xy} \end{Bmatrix}; \qquad (9)$$

Q_{ij} $(i, j = 1, \ldots, 6)$ are the elastic coefficients calculated as follows:

$$Q_{11}(z) = Q_{22}(z) = Q_{33}(z) = \frac{E(z)(1-\upsilon)}{(1-2\upsilon)(1+\upsilon)},$$
$$Q_{12}(z) = Q_{13}(z) = Q_{23}(z) = \frac{E(z)\upsilon}{(1-2\upsilon)(1+\upsilon)}, \qquad (10)$$
$$Q_{44}(z) = Q_{55}(z) = Q_{66}(z) = \frac{E(z)}{2(1+\upsilon)}.$$

The governing equations for porous FG plates on elastic foundations are derived using Hamilton's principle. They mathematically represent bending and vibration behaviours:

$$\int_0^t \left(\delta U_{\mathrm{P}} + \delta U_{\mathrm{F}} + \delta V - \delta K\right) dt = 0\,. \qquad (11)$$

The expressions mentioned represent modifications of the elastic strain energy δU_{P}, the elastic strain energy associated with the foundation δU_{F}, the potential energy due to external loads δV, and the variation of the kinetic energy of the plate δK.

A detailed explanation of these energy variations is provided in the following sections:

$$\delta U_{\mathrm{P}} = \int_{\Delta} \int_{-h/2}^{h/2} (\sigma_{xx}\delta\varepsilon_{xx} + \sigma_{yy}\delta\varepsilon_{yy} + \sigma_{zz}\delta\varepsilon_{zz} + \tau_{xz}\delta\gamma_{xz} + \tau_{yz}\delta\gamma_{yz} + \tau_{xy}\delta\gamma_{xy}) dz\, d\Delta\,, \qquad (12)$$

$$\delta U_{\mathrm{F}} = \int_{\Delta} \left\{ k_{\mathrm{w}} u_3^2 - k_{\mathrm{s}} \left(\left(\frac{\partial u_3}{\partial x} \right)^2 + \left(\frac{\partial u_3}{\partial y} \right)^2 \right) \right\} \delta u_3\, d\Delta\,, \qquad (13)$$

$$\delta V = \int_{\Delta} q\, \delta u_3\, d\Delta\,, \qquad (14)$$

$$\delta K = \int_{\Delta} \int_{-h/2}^{h/2} \rho(\dot{u}_1 \delta\dot{u}_1 + \dot{u}_2 \delta\dot{u}_2 + \dot{u}_2 \delta\dot{u}_2) dz\, d\Delta\,. \qquad (15)$$

$\delta u_{0.2}$, $\delta u_{0.3}$, $\delta u_{0.4}$ to zero:

$$\begin{aligned}
&\delta u_{0.1}: \quad \frac{\partial N_{xx}}{\partial x}+\frac{\partial N_{xy}}{\partial y}=T_0\ddot{u}_{0.1}-T_1\frac{\partial \ddot{u}_{0.3}}{\partial x}+T_3\frac{\partial \ddot{u}_{0.4}}{\partial x},\\
&\delta u_{0.2}: \quad \frac{\partial N_{xy}}{\partial x}+\frac{\partial N_{yy}}{\partial y}=T_0\ddot{u}_{0.2}-T_1\frac{\partial \ddot{u}_{0.3}}{\partial y}+T_3\frac{\partial \ddot{u}_{0.4}}{\partial y},\\
&\delta u_{0.3}: \quad \frac{\partial^2 M_{xx}}{\partial x^2}+2\frac{\partial^2 M_{xy}}{\partial x\partial y}+\frac{\partial^2 M_{yy}}{\partial y^2}-k_{\mathrm{w}}u_{0,3}+k_{\mathrm{s}}\left(\frac{\partial^2 u_{0.3}}{\partial x^2}+\frac{\partial^2 u_{0.3}}{\partial y^2}\right)=T_0\ddot{u}_{0.3}+\\
&+T_1\left(\frac{\partial \ddot{u}_{0.1}}{\partial x}+\frac{\partial \ddot{u}_{0.2}}{\partial y}\right)-T_2\left(\frac{\partial^2 \ddot{u}_{0.3}}{\partial x^2}+\frac{\partial^2 \ddot{u}_{0.3}}{\partial y^2}\right)+T_4\left(\frac{\partial^2 \ddot{u}_{0.4}}{\partial x^2}+\frac{\partial^2 \ddot{u}_{0.4}}{\partial y^2}\right)+T_6\ddot{u}_{0.4},\\
&\delta u_{0.4}: \quad \frac{\partial^2 S_{xx}}{\partial x^2}+2\frac{\partial^2 S_{xy}}{\partial x\partial y}+\frac{\partial^2 S_{yy}}{\partial y^2}+N_{zz}-\frac{\partial Q_{xz}}{\partial x}-\frac{\partial Q_{yz}}{\partial y}=\\
&=T_3\left(\frac{\partial \ddot{u}_{0.1}}{\partial x}+\frac{\partial \ddot{u}_{0.2}}{\partial y}\right)-T_4\left(\frac{\partial^2 \ddot{u}_{0.3}}{\partial x^2}+\frac{\partial^2 \ddot{u}_{0.3}}{\partial y^2}\right)+T_5\left(\frac{\partial^2 \ddot{u}_{0.4}}{\partial x^2}+\frac{\partial^2 \ddot{u}_{0.4}}{\partial y^2}\right)-T_6\ddot{u}_{0.3}-T_7\ddot{u}_{0.4},
\end{aligned} \tag{16}$$

wherein N_{ij}, M_{ij}, S_{ij}, Q_{iz}, N_{zz}, and T_i ($i = 0, \ldots, 7$) are defined as follow:

$$[N_{ij}, M_{ij}, S_{ij}] = \int_{-h/2}^{h/2} [1, z, \Phi(z)]\sigma_{ij} dz \ (i, j = x, y), \tag{17}$$

$$Q_{ij} = \int_{-h/2}^{h/2} \left(\frac{\partial \Phi(z)}{\partial z} + \Gamma(z)\right)\tau_{ij} dz \ (i, j = x, y), \tag{18}$$

$$N_{zz} = \int_{-h/2}^{h/2} \left(\frac{\partial \Gamma(z)}{\partial z}\right)\sigma_{zz} dz, \tag{19}$$

$$\begin{aligned}
&\{T_0, T_1, T_2, T_3, T_4, T_5, T_6, T_7\} =\\
&= \int_{-h/2}^{h/2} \rho\{1, z, z^2, \Phi(z), z\Phi(z), \Phi^2(z), \Gamma(z), \Gamma^2(z)\} dz.
\end{aligned} \tag{20}$$

3. NAVIER SOLUTION TECHNIQUE

This study investigates simply supported rectangular FG plates. The plates are subject to the following boundary conditions:

$$\begin{aligned}
&u_{0.1} = u_{0.3} = u_{0.4} = N_{xx} = M_{xx} = S_{xx} = N_{zz} = 0 \text{ at } x = 0,\ a,\\
&u_{0.2} = u_{0.3} = u_{0.4} = N_{yy} = M_{yy} = S_{yy} = N_{zz} = 0 \text{ at } y = 0,\ b.
\end{aligned} \tag{21}$$

The Navier solution method can be employed to obtain an analytical solution to the governing Eqs. (16) by assuming the following forms for the unknown quantities $u_{0.1}$, $u_{0.2}$, $u_{0.3}$, $u_{0.4}$, and q:

$$u_{0.1} = \sum_{m=1}^{\infty}\sum_{n=1}^{\infty} U_1^{mn} e^{i\omega_{mn}t} \cos(\lambda x)\sin(\mu y),$$

$$u_{0.2} = \sum_{m=1}^{\infty}\sum_{n=1}^{\infty} U_2^{mn} e^{i\omega_{mn}t} \sin\lambda x \cos(\mu y),$$

$$u_{0.3} = \sum_{m=1}^{\infty}\sum_{n=1}^{\infty} U_3^{mn} e^{i\omega_{mn}t} \sin(\lambda x)\sin(\mu y), \tag{22}$$

$$u_{0.4} = \sum_{m=1}^{\infty}\sum_{n=1}^{\infty} U_4^{mn} e^{i\omega_{mn}t} \sin(\lambda x)\sin(\mu y),$$

$$q = \sum_{m=1}^{\infty}\sum_{n=1}^{\infty} q_{mn} \sin(\lambda x)\sin(\mu y);$$

$U_1^{mn}, U_2^{mn}, U_3^{mn}, U_4^{mn}$ are coefficients to be determined, and the eigen frequency ω_{mn} is associated with (m, n) eigen mode. Substituting Eqs. (22) into Eqs. (16) yields the algebraic equations written in matrix form:

$$\left(\begin{bmatrix} k_{11} & k_{12} & k_{13} & k_{14} \\ k_{12} & k_{22} & k_{23} & k_{24} \\ k_{13} & k_{23} & k_{33} & k_{34} \\ k_{14} & k_{24} & k_{34} & k_{44} \end{bmatrix} - \begin{bmatrix} m_{11} & 0 & m_{13} & m_{14} \\ 0 & m_{22} & m_{23} & m_{24} \\ m_{13} & m_{23} & m_{33} & m_{34} \\ m_{14} & m_{24} & m_{34} & m_{44} \end{bmatrix} \omega_{mn}^2 \right) \begin{Bmatrix} U_1^{mn} \\ U_2^{mn} \\ U_3^{mn} \\ U_4^{mn} \end{Bmatrix} = \begin{Bmatrix} 0 \\ 0 \\ q_{mn} \\ 0 \end{Bmatrix} \tag{23}$$

with

$$k_{11} = A_{11}\lambda^2 + A_{66}\mu^2,\ k_{12} = (A_{12} + A_{66})\lambda\mu,\ k_{13} = -B_{11}\lambda^3 - (B_{12} + 2B_{66})\lambda\mu^2,$$
$$k_{14} = -H_{13}\lambda + C_{11}\lambda^3 + (C_{12} + 2C_{66})\lambda\mu^2,\ k_{22} = A_{66}\lambda^2 + A_{22}\mu^2,$$
$$k_{23} = -(B_{12} + 2B_{66})\lambda^2\mu - B_{22}\mu^3,\ k_{24} = -H_{23}\mu + (C_{12} + 2C_{66})\lambda^2\mu + C_{22}\mu^3,$$
$$k_{33} = D_{11}(\lambda^4 + \mu^4) + 2(D_{12} + 2D_{66})\lambda^2\mu^2 + k_w + k_s(\lambda^2 + \mu^2), \tag{24}$$
$$k_{34} = I_{13}(\lambda^2 + \mu^2) - F_{11}(\lambda^4 + \mu^4) - 2(F_{12} + 2F_{66})\lambda^2\mu^2,$$
$$k_{44} = L_{33} + (\lambda^2 + \mu^2)(K_{44} - 2J_{13}) + G_{11}(\lambda^4 + \mu^4) + 2(G_{12} + 2G_{66})\lambda^2\mu^2,$$
$$m_{11} = m_{22} = T_0,\ m_{13} = -T_1\lambda,\ m_{14} = T_3\lambda,\ m_{23} = -T_1\mu,\ m_{24} = T_3\mu,$$
$$m_{33} = T_0 + T_2(\lambda^2 + \mu^2),\ m_{34} = T_6 - T_4(\lambda^2 + \mu^2),\ m_{44} = T_7 - T_5(\lambda^2 + \mu^2).$$

4. NUMERICAL RESULTS AND DISCUSSION

4.1. Comparison and Validation Study

In this section, we conduct a thorough comparison and validation study centred on the dynamic behaviour analysis characteristics of

TABLE 1. The properties of the materials.

Material	Properties	
	E, GPa	ρ, kg/m^3
Aluminium (Al)	70	2702
Alumina (Al_2O_3)	380	3800

functionally graded plates. Non-dimensional fundamental frequencies predicted using the current power-law, four-parameter Viola–Tornabene, and trigonometric models are benchmarked against published literature values. Four different patterns of porosity variations are applied to analyse further the present approaches by comparing our results with work of Addou *et al.* [4].

The material properties of the functionally graded materials employed in this study are listed in Table 1.

The results align well with previous studies, validating the accuracy. This analysis confirms the method's reliability and potential impact, demonstrating its ability to capture the effects of geometric ratios and material gradation on FG plate vibration characteristics. The proposed model proves valuable for understanding and optimizing FGM structures.

4.2. Parametric Study and Effect of Porous Coefficient ϕ on the Non-Dimensional Fundamental Frequencies

Figures 3 and 4 illustrate the impact of porous coefficient ϕ on the non-dimensional fundamental frequencies ω response of a functionally graded Al/Al_2O_3 plate (gradient index $\Delta = 1$). The study explores the influence of three different models for distributing material volume fractions through the plate thickness: power-law model, Viola–Tornabene four-parameter model, and trigonometric model are further compared across four different models for porosity conditions are considered: perfect, even porosity, uneven porosity, logarithmic-uneven porosity and mass-density porosity each with varying porosity coefficients ($\phi = 0$–0.05–0.10–0.15–0.20).

Regarding the material volume fraction distribution models, the Viola–Tornabene four-parameter profile leads to the maximum $\overline{\omega}$ values followed by the power-law and finally the trigonometric model, which shows the minimum frequencies. Moreover, the impact of mass-density distributed porosities is greater followed by uneven distributed porosities and logarithmic-uneven distributed porosities respectively, than the even distributed porosities which shows the minimum frequencies.

It is important to note that an increase in the porosity coefficients ϕ leads to an increase in the non-dimensional fundamental frequencies $\bar{\omega}$ except in the even distributed porosities, which shows a decrease of frequencies with the increase in the porosity coefficients ϕ.

The findings indicate that within the patterns of porosity variations, the mass-density distributed porosities consistently yields the highest

TABLE 2. Comparison of the non-dimensional fundamental frequencies of square plate with $\Delta = 1$.

h/a	Model	ϕ	Even porosity	Uneven porosity	Logarithmic-uneven porosity	Mass-density porosity	Perfect
0.05	Power-law [4], Voigt	0.05	8.8888	9.0368	9.0368	8.6248	9.030
		0.10	8.7352	9.0456	9.0456	8.1224	
		0.15	8.5656	9.0552	9.0544	7.4713	
		0.20	8.3728	9.0656	9.0640	6.5652	
	Power-law (present), Voigt	0.05	8.9471	9.1716	9.0527	9.2585	9.0240
		0.10	8.8555	9.3317	9.0810	9.5123	
		0.15	8.7451	9.5062	9.1089	9.7882	
		0.20	8.6100	9.6973	9.1363	10.0895	
	Viola–Tornabene four-parameter (present), Voigt	0.05	11.1603	11.3145	11.1756	11.3682	9.0240
		0.10	11.2304	11.5503	11.2560	11.6610	
		0.15	11.3075	11.8066	11.3375	11.9777	
		0.20	11.3927	12.0861	11.4202	12.3216	
	Trigonometric (present), Voigt	0.05	7.7670	8.0537	7.9407	8.1672	7.9430
		0.10	7.5512	8.1736	7.9360	8.4117	
		0.15	7.2799	8.3038	7.9286	8.6794	
		0.20	6.9275	8.4458	7.9181	8.9745	
0.10	Power-law [4], Voigt	0.05	8.6992	8.8408	8.8402	8.4432	8.836
		0.10	8.5520	8.8464	8.8458	7.9568	
		0.15	8.3898	8.8532	8.8526	7.3262	
		0.20	8.2058	8.8606	8.8594	6.4470	
	Power-law (present), Voigt	0.05	8.7498	8.9649	8.8483	9.0523	8.8229
		0.10	8.6627	9.1190	8.8732	9.3007	
		0.15	8.5575	9.2870	8.8977	9.5706	
		0.20	8.4287	9.4710	8.9215	9.8655	
	Viola–Tornabene four-parameter (present), Voigt	0.05	10.8413	10.9878	10.8527	11.0453	10.7812
		0.10	10.9072	11.2112	10.9250	11.3297	
		0.15	10.9796	11.4537	10.9982	11.6373	
		0.20	11.0597	11.7180	11.0723	11.9714	

Continuation of Table 2.

		0.05	7.5845	7.8586	7.7480	7.9731	
		0.10	7.3767	7.9716	7.7393	8.2119	
	Trigonometric (present), Voigt	0.15	7.1156	8.0942	7.7277	8.4735	
		0.20	6.7764	8.2278	7.7127	8.7617	7.7540
		0.10	7.1168	7.6727	7.4483	7.9150	
		0.15	6.8704	7.7847	7.4313	8.1673	
		0.20	6.5502	7.9067	7.4107	8.4455	
		0.05	8.0635	8.1795	8.1795	7.8280	
	Power-law [4], Voigt	0.10	7.9385	8.1800	8.1800	7.3930	8.180
		0.15	7.8015	8.1815	8.1810	6.8285	
		0.20	7.6450	8.1835	8.1830	6.0395	
		0.05	8.0966	8.2831	8.1743	8.3708	
	Power-law (present), Voigt	0.10	8.0231	8.4186	8.1897	8.6009	8.1582
		0.15	7.9341	8.5663	8.2044	8.8511	
		0.20	7.8247	8.7282	8.2184	9.1245	
0.20	Viola–Tornabene four-parameter (present), Voigt	0.05	9.8296	9.9537	9.8309	10.0199	
		0.10	9.8834	10.1408	9.8814	10.2778	
		0.15	9.9426	10.3436	9.9321	10.5567	9.7804
		0.20	10.0079	10.5643	9.9829	10.8596	
		0.05	6.9870	7.2228	7.1203	7.3385	
	Trigonometric (present), Voigt	0.10	6.8041	7.3157	7.1011	7.5586	7.1365
		0.15	6.5747	7.4162	7.0786	7.7999	
		0.20	6.2767	7.5253	7.0524	8.0658	

estimates for the non-dimensional fundamental frequencies $\bar{\omega}$, followed by the uneven distributed porosities and logarithmic-uneven distributed porosities respectively, while the even distributed porosities provide the lowest predictions.

Concerning the models describing material volume-fraction distribution, the Viola–Tornabene four-parameter profile produces the maximum values for non-dimensional fundamental frequencies ω, followed by the power-law model, with the trigonometric model exhibiting the minimum frequencies.

As the value of the porous coefficient, ϕ increases, there is a rapid increase in non-dimensional fundamental frequencies ω, except in the even distributed porosities in the power-law model and the trigonometric model, which shows a decrease of frequencies with the increase in the porosity coefficients ϕ.

Figures 5 and 6 illustrates the impact of thickness-to-span ratio h/a on the non-dimensional fundamental frequencies ω response of a functionally graded Al/Al_2O_3 plate (gradient index $\Delta = 1$) and porosity coefficients ($\phi = 0.10$). The study explores the influence of three different

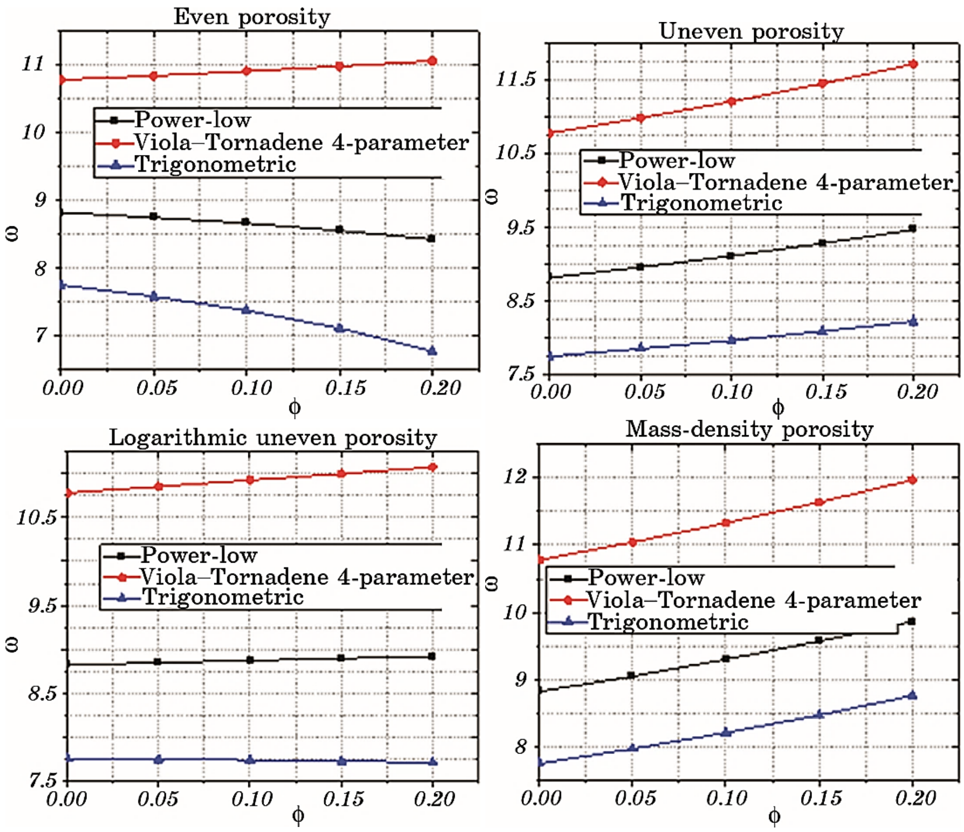

Fig. 3. Effect of porous coefficient ϕ on the non-dimensional fundamental frequencies for Al/Al_2O_3-interface plate with different homogenization models ($\Delta = 1$, $h/a = 0.1$).

models for distributing material volume fractions through the plate thickness: power-law model, Viola–Tornabene four-parameter model, and trigonometric model and further compared across four different models for porosity conditions are considered: Perfect, even porosity, uneven porosity, logarithmic-uneven porosity and mass-density porosity each with varying porosity coefficients ($\phi = 0$–0.05–0.10–0.15–0.20).

The results of Figure 5 demonstrate clear trends in fundamental frequency predictions across the different modelling approaches. The Viola–Tornabene four-parameter distribution model produces the highest frequencies, followed by power-law model, while trigonometric model give identical lower estimates. For the different patterns of porosity variations, the mass-density distributed porosities yields maximum frequencies, followed by the uneven distributed porosities and

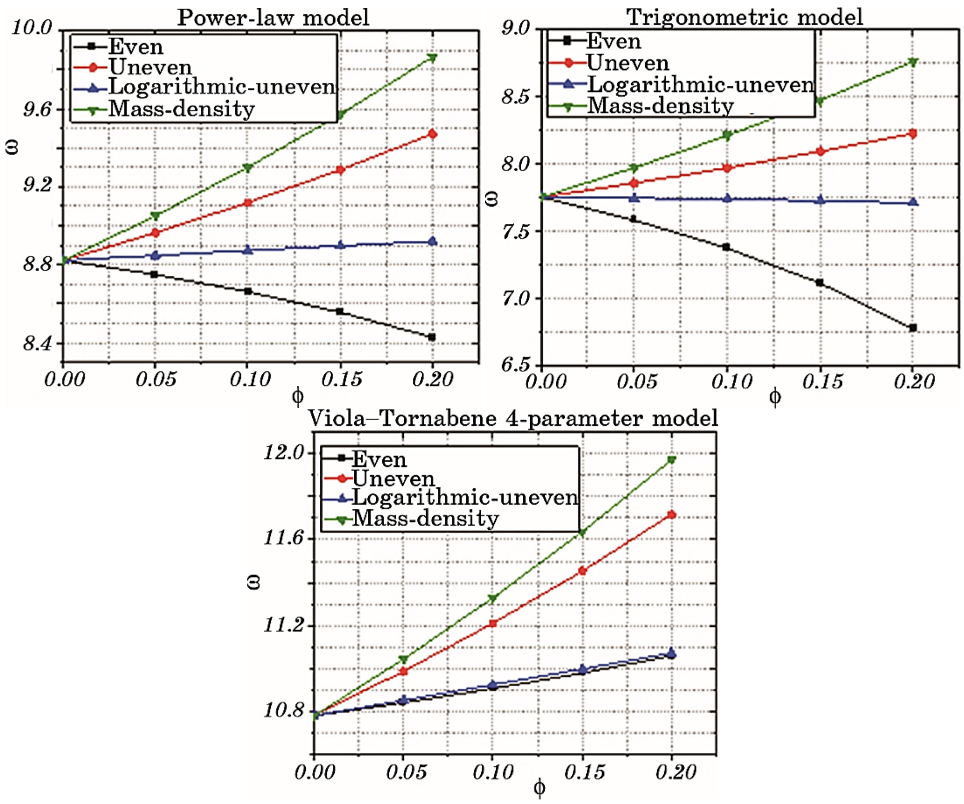

Fig. 4. Effect of porous coefficient ϕ on the non-dimensional fundamental frequencies for Al/Al_2O_3-interface square plate with different patterns of porosity variations ($\Delta = 1$, $h/a = 0.1$, $k_s^m = k_w^m = 0$).

logarithmic-uneven distributed porosities respectively and even distributed porosities the minimum. A distinct effect of increasing thickness-to-span ratio h/a is observed, with a rapid decline in non-dimensional fundamental frequencies as the index grows. This h/a-dependent reduction occurs irrespective of the model utilized.

The findings indicate that within the different patterns of porosity variations models, the mass-density distributed porosities consistently yields the highest estimates for non-dimensional fundamental frequencies ω, followed by the uneven distributed porosities and logarithmic-uneven distributed porosities, while the even distributed porosities provide the lowest and predictions.

Concerning the models describing material volume-fraction distribution, the Viola–Tornabene four-parameter profile produces the maximum values for non-dimensional fundamental frequencies ω, followed by the power-law model, with the trigonometric model exhibiting the

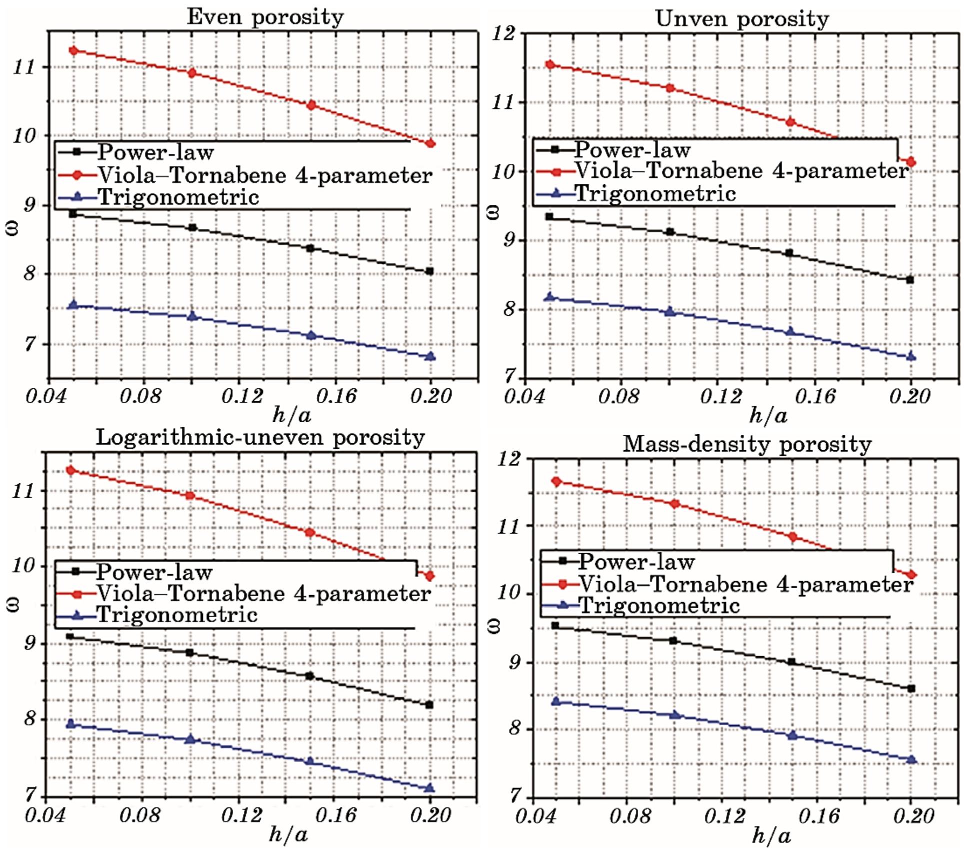

Fig. 5. Effect of thickness-to-span ratio h/a on the non-dimensional fundamental frequencies for Al/Al_2O_3-interface plate with different homogenization models ($\Delta = 1$, $\phi = 0.1$).

minimum deflection.

As the thickness-to-span ratio h/a increases, there is a corresponding decrease in the non-dimensional fundamental frequencies ω.

5. CONCLUSION

This study presents a comprehensive analysis of the dynamic responses of porous functionally graded Al/Al_2O_3 plates using various homogenization models and material distribution profiles. The following key conclusions can be drawn.

1. The Viola–Tornabene four-parameter model consistently produces the highest non-dimensional fundamental frequencies, followed by the power-law model, while the trigonometric model yields the lowest fre-

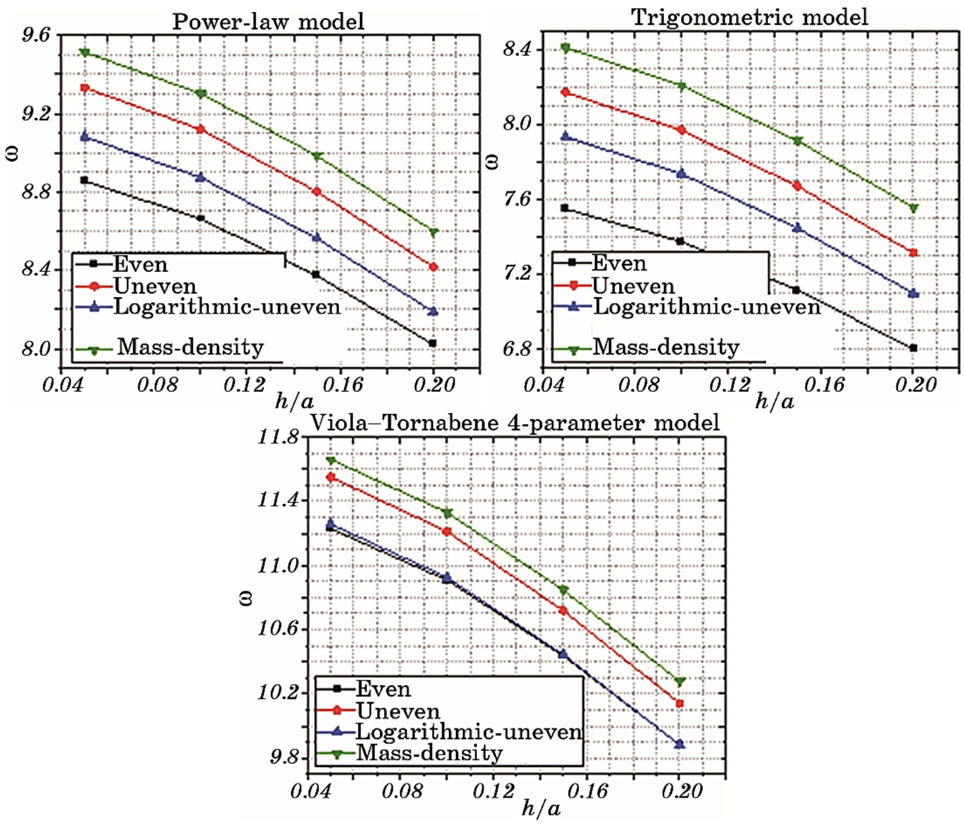

Fig. 6. Effect of thickness-to-span ratio h/a on the non-dimensional fundamental frequencies for Al/Al_2O_3-interface plate with different patterns of porosity variations ($\Delta = 1$, $\phi = 0.1$).

quencies across all porosity patterns.
2. Among the porosity variation patterns, mass-density distributed porosities result in the maximum frequencies, followed by uneven and logarithmic-uneven distributions, with even porosity distribution showing the minimum frequencies.
3. Increasing the porosity coefficient generally leads to an increase in non-dimensional fundamental frequencies, except in the case of evenly distributed porosities, which shows a decrease in frequencies with increasing porosity.
4. The thickness-to-span ratio has a significant impact on the dynamic response, with increasing ratios resulting in a rapid decline in non-dimensional fundamental frequencies across all models and porosity patterns.
5. The proposed analytical model demonstrates good agreement with previous studies, validating its accuracy and reliability for predicting

the dynamic behaviour of porous FGM plates.

These findings provide valuable insights for the design and optimization of functionally graded porous plates in various engineering applications. The results can be used to tailor the dynamic properties of FGM structures by selecting appropriate material gradation profiles, porosity patterns, and geometric parameters. Future work could explore the effects of different boundary conditions, thermal loads, and more complex geometries on the dynamic behaviour of porous FGM plates.

This work was supported by the University research and training projects (PRFU), code A01L02UN220120200004, which provide essential support for doctoral training in higher education institutions in Algeria.

REFERENCES

1. M. Naebe and K. Shirvanimoghaddam, *Appl. Mater. Today*, **5**: 223 (2016).
2. J. Zhu, Z. Lai, Z. Yin, J. Jeon, and S. Lee, *Mater. Chem. Phys.*, **68**: 130 (2001).
3. N. Wattanasakulpong, B. G. Prusty, D. W. Kelly, and M. Hoffman, *Mater. Design*, **36**: 182 (2012).
4. F. Y. Addou, M. Meradjah, A. A. Bousahla, A. Benachour, F. Bourada, A. Tounsi, and S. R. Mahmoud, *Computers and Concrete*, **24**, Iss. 4: 347 (2019).
5. F. Z. Zaoui, D. Ouinas, B. Achour, M. Touahmia, M. Boukendakdji, E. R. Latifee, and J. A. Vica Olay, *Mathematics*, **10**: 4764 (2022).
6. B. Damani, A. Fekrar, M. M. Selim, K. H. Benrahou, A. Benachour, A. Tounsi, and M. Hussain, *Struct. Eng. Mech.*, **78**: 439 (2021).
7. S. Merdaci, H. M. Adda, B. Hakima, R. Dimitri, and F. Tornabene, *J. Compos. Sci.*, **5**: 305 (2021).
8. A. Mahmoudi, R. Bachir-Bouiadjra, S. Benyoucef, and A. Tounsi, *Nature Technol.*, **17**: (2017).
9. A. Berkia, B. Rebai, B. Litouche, S. Abbas, and K. Mansouri, *AIMS Mater. Sci.*, **10**, Iss. 5: 891 (2023).
10. R. Billel, *AIMS Mater. Sci.*, **10**, Iss. 1: 26 (2023).
11. H. Benaddi, B. Rebai, K. Mansouri, N. M. Seyam, and A. M. Zenkour, *J. Comput. Appl. Mech.*, **55**, Iss. 3: 369 (2024).
12. Z. Yin, H. Gao, and G. Lin, *Eng. Analysis Boundary Elements*, **133**: 185 (2021).
13. Y. S. Al Rjoub and J. A. Alshatnawi, *Structures*, **28**: 2392 (2020).
14. X. Hu and T. Fu, *J. Mech. Sci. Technol.*, **37**: 5725 (2023).
15. M. Kaddari, A. Kaci, A. A. Bousahla, A. Tounsi, F. Bourada, E. A. Bedia, and M. A. Al-Osta, *Computers and Concrete*, **25**, Iss. 1: 37 (2020).
16. N. Sharma, P. Tiwari, D. K. Maiti, and D. Maity, *Composites Part C*, **6**: 100208 (2021).
17. S. K. Sah and A. Ghosh, *Composite Structures*, **279**: 114795 (2022).
18. V. Kumar, S. J. Singh, V. H. Saran, and S. P. Harsha, *Eur. J. Mech. A/Solids*, **85**: 104124 (2021).
19. V. Kumar, S. J. Singh, V. H. Saran, and S. P. Harsha, *Int. J. Struct. Stab. Dyn.*, **23**: 2350024 (2023).
20. D. Shahsavari, M. Shahsavari, L. Li, and B. Karami, *Aerosp. Sci. Technol.*, **72**:

134 (2018).
21. M. Arefi, M. Kiani, and A. M. Zenkour, *J. Sandwich Struct. Mater.*, **22**: 55 (2020).
22. W. Y. Jung, W. T. Park, and S. C. Han, *Int. J. Mech. Sci.*, **87**: 150 (2014).
23. L. L. Ke, J. Yang, S. Kitipornchai, and M. A. Bradford, *Composite Structures*, **94**: 3250 (2012).
24. K. Magnucki and P. Stasiewicz, *J. Theor. Appl. Mech.*, **42**: 859 (2004).
25. N. Wattanasakulpong and V. Ungbhakorn, *Aerospace Sci. Technol.*, **32**, Iss. 1: 111 (2014).
26. D. Chen, J. Yang, and S. Kitipornchai, *Composite Structures*, **133**: 54 (2015).
27. D. Chen, S. Kitipornchai, and J. Yang, *Thin-Walled Structures*, **107**: 39 (2016).
28. M. Jabbari, A. Mojahedin, A. Khorshidvand, and M. Eslami, *J. Eng. Mech.*, **140**: 287 (2014).
29. A. Mojahedin, E. F. Joubaneh, and M. Jabbari, *Acta Mech.*, **225**: 3437 (2014).
30. T. Yu, T. Q. Bui, S. Yin, D. H. Doan, C. Wu, T. Van Do, and S. Tanaka, *Composite Structures*, **136**: 684 (2016).
31. F. Mouaici, S. Benyoucef, H. A. Atmane, and A. Tounsi, *Wind Struct.*, **22**: 429 (2016).